

A modified Marchenko method to retrieve the wave field inside layered metamaterial from reflection measurements at the surface

Kees Wapenaar^{a)}

Department of Geoscience and Engineering, Delft University of Technology, Stevinweg 1, 2628 CN Delft, The Netherlands

ABSTRACT:

With the Marchenko method, it is possible to retrieve the wave field inside a medium from its reflection response at the surface. To date, this method has predominantly been applied to naturally occurring materials. This study extends the Marchenko method for applications in layered metamaterials with, in the low-frequency limit, effective negative constitutive parameters. It illustrates the method with a numerical example, which confirms that the method properly accounts for multiple scattering. The proposed method has potential applications, for example, in non-destructive testing of layered materials. © 2020 Acoustical Society of America. <https://doi.org/10.1121/10.0001761>

(Received 20 May 2020; revised 22 July 2020; accepted 27 July 2020; published online 24 August 2020)

[Editor: Olga Umnova]

Pages: 939–953

I. INTRODUCTION

Building on classical inverse scattering theory,^{1–4} recent research has opened new ways of retrieving the wave field inside a medium from its reflection response at the surface^{5–13} and using this for imaging.^{14–22} These methods, named after Marchenko,¹ have in common that they account for multiple scattering inside the medium and yet require only a single-sided reflection response as input, together with a background model of the medium.

The Marchenko method has almost exclusively been applied to naturally occurring materials (with the exception of an application to non-reciprocal materials²³), but it has not yet been applied to metamaterials with, in the low-frequency limit, effective negative constitutive parameters. A classical reference on wave propagation in materials with negative permittivity and permeability is the paper by Veselago,²⁴ in which it is shown that such materials exhibit negative refraction. Since the discovery by Pendry²⁵ that negative refraction makes a perfect lens, there has been a significant interest in electromagnetic wave propagation in metamaterials.^{26–34} Almost simultaneously, after the first fabrication of an elastic metamaterial with effective negative elastic parameters,³⁵ much research has been directed toward wave propagation in elastic metamaterials.^{36–45}

Here, we modify the Marchenko method for metamaterials. We start by formulating a wave equation that holds for elastodynamic and electromagnetic waves in natural materials and metamaterials. We show that metamaterials, with negative phase slowness and positive group slowness, are by definition dispersive. This implies that a modification of the standard Marchenko method is needed. Next, we derive wave field representations for a layered medium, consisting

of a mix of natural materials and metamaterials. Using these representations, we derive the Marchenko method for such a medium. This method uses new window functions that better acknowledge the dispersive behaviour of waves propagating through metamaterial. We conclude by illustrating the modified Marchenko method with a numerical example.

II. WAVE EQUATION FOR NATURAL MATERIALS AND METAMATERIALS

A. Basic equations

Throughout this paper, we consider scalar wave propagation in the two-dimensional (2D) plane. This allows for capturing of different wave phenomena by a unified wave equation. We define the Cartesian coordinate vector in the 2D plane as $\mathbf{x} = (x_1, x_3)$, where positive x_3 denotes depth in a horizontally layered medium. Quantities that are a function of space and time are denoted as $u(\mathbf{x}, t)$, where t stands for time. We define the temporal Fourier transform of $u(\mathbf{x}, t)$ as

$$u(\mathbf{x}, \omega) = \int_{-\infty}^{\infty} u(\mathbf{x}, t) \exp(i\omega t) dt, \quad (1)$$

where ω is the angular frequency and i the imaginary unit. For convenience, quantities in the time and frequency domain are denoted by the same symbol (here u). The inverse Fourier transform is defined as

$$u(\mathbf{x}, t) = \frac{1}{2\pi} \int_{-\infty}^{\infty} u(\mathbf{x}, \omega) \exp(-i\omega t) d\omega. \quad (2)$$

Throughout this paper, quantities in the time domain are real-valued, hence Eq. (1) implies $u(\mathbf{x}, -\omega) = u^*(\mathbf{x}, \omega)$, where the asterisk denotes complex conjugation. Using this property, the inverse Fourier transform can be rewritten as

^{a)}Electronic mail: C.P.A.Wapenaar@TUDelft.NL, ORCID: 0000-0002-1620-8282.

$$u(\mathbf{x}, t) = \frac{1}{\pi} \Re \int_0^\infty u(\mathbf{x}, \omega) \exp(-i\omega t) d\omega, \quad (3)$$

where \Re denotes that the real part is taken. Since the integral is taken over positive frequencies only, it is sufficient to restrict our derivations in the frequency domain to positive frequencies. This avoids complications related to the sign of the frequency.

In the space-frequency domain, we consider the following system of equations in the low-frequency limit for 2D wave propagation in an inhomogeneous, transverse isotropic natural material, or metamaterial:

$$-i\omega\alpha P + \partial_1 Q_1 + \partial_3 Q_3 = B, \quad (4)$$

$$-i\omega\beta_1 Q_1 + \partial_1 P = C_1, \quad (5)$$

$$-i\omega\beta_3 Q_3 + \partial_3 P = C_3. \quad (6)$$

These equations hold for acoustic (AC), horizontally polarised shear (SH), transverse-electric (TE), and transverse-magnetic (TM) wave fields. Operator ∂_i stands for the partial differential operator $\partial/\partial x_i$. The wave fields $[P(\mathbf{x}, \omega)$ and $Q_i(\mathbf{x}, \omega)]$ and sources $[B(\mathbf{x}, \omega)$ and $C_i(\mathbf{x}, \omega)]$ are space- and frequency-dependent macroscopic quantities. These are often denoted as $\langle P \rangle$, etc.,³³ but for notational convenience we will not use the brackets. The medium parameters $[\alpha(x_3, \omega)$ and $\beta_i(x_3, \omega)]$ are effective parameters (which, in a layered medium, are varying in the x_3 -direction only). At layer interfaces, where the medium parameters are discontinuous, the boundary conditions state that the wave field quantities P and Q_3 are continuous. The wave fields, sources, and medium parameters are specified for the different wave phenomena in Table I. For AC and SH waves, p is the acoustic pressure, τ_{ij} the stress, v_i the particle velocity, κ the compressibility, ρ_{ij} the mass density, s_{ijkl} the compliance, q the volume injection-rate density, F_i the external force density, and h_{ij} the external deformation-rate density. For TE and TM waves, E_i is the electric field strength, H_i the magnetic field strength, ϵ_{ij} the permittivity, μ_{ij} the permeability, J_i^e the external electric current density, and J_i^m the external magnetic current density.

For natural materials, the real parts of the medium parameters α and β_i are positive (and the imaginary parts are positive or zero). Such a medium will be called a double-positive (DPS) medium.³⁰ For metamaterials, the real part of one or more of the medium parameters is negative. When both α and β_i have negative real parts, we speak of a double-negative (DNG) medium.³⁰ The phase slowness of a DNG

medium is negative,²⁴ see also Sec. IID. To obey causality, the group slowness should be positive. These opposite slownesses imply that the parameters of a DNG medium are frequency-dependent and complex-valued (with positive imaginary parts).²⁸ The inherent dispersive character of DNG media implies that the Marchenko method needs to be modified for such media (see Sec. IV).

In the following, we separate the space- and frequency-dependency of the medium parameters for DPS as well as DNG media according to

$$\alpha(x_3, \omega) = \alpha_0(x_3)h_\alpha(\omega), \quad (7)$$

$$\beta_i(x_3, \omega) = \beta_{i,0}(x_3)h_\beta(\omega), \quad (8)$$

with positive real-valued $\alpha_0(x_3)$ and $\beta_{i,0}(x_3)$. For DNG media, an often used model for the frequency-dependent functions is the Drude model,²⁶ where

$$h_\alpha(\omega) = 1 - \frac{\omega_\alpha^2}{\omega(\omega + i\Gamma_\alpha)}, \quad (9)$$

$$h_\beta(\omega) = 1 - \frac{\omega_\beta^2}{\omega(\omega + i\Gamma_\beta)}, \quad (10)$$

with small positive real-valued Γ_α and Γ_β . Note that $\Re(h_\alpha) < 0$ for $\omega^2 < \omega_\alpha^2 - \Gamma_\alpha^2$ and $\Im(h_\alpha) > 0$ (where \Im denotes the imaginary part) for all positive ω . Similar properties hold for h_β . Hence, in the low-frequency limit, these parameters obey the mentioned conditions for a DNG medium. In Sec. IIE, we confirm that the group slowness for this type of DNG medium is positive.

In the following, we assume that the medium parameters (for DPS and DNG media) are defined by the more general relations [Eqs. (7) and (8)]. Whenever we use the Drude model for DNG media [Eqs. (9) and (10)], we mention this explicitly.

B. Matrix-vector wave equation

We reorganise the basic Eqs. (4)–(6) into a matrix-vector wave equation. This wave equation is a suited starting point for the derivation of representations for the Marchenko method in Sec. III.

We define the spatial Fourier transform of a function $u(x_1, x_3, \omega)$ as

$$\tilde{u}(s_1, x_3, \omega) = \int_{-\infty}^{\infty} u(x_1, x_3, \omega) \exp(-i\omega s_1 x_1) dx_1, \quad (11)$$

with s_1 being the horizontal slowness. This transformation accomplishes a decomposition of the wave field $u(x_1, x_3, \omega)$ into plane-wave components $\tilde{u}(s_1, x_3, \omega)$. We use Eq. (11) to transform Eqs. (4)–(6) from the space-frequency domain (x_1, x_3, ω) to the slowness-depth-frequency domain (s_1, x_3, ω) . Differentiations with respect to x_1 thus become multiplications by $i\omega s_1$. Eliminating \tilde{Q}_1 from the

TABLE I. Quantities in Eqs. (4)–(6).

	P	Q_1	Q_3	α	β_1	β_3	B	C_1	C_3
AC	p	v_1	v_3	κ	ρ_{11}	ρ_{33}	q	F_1	F_3
SH	v_2	$-\tau_{21}$	$-\tau_{23}$	ρ_{22}	$4s_{1221}$	$4s_{3223}$	F_2	$2h_{21}$	$2h_{23}$
TE	E_2	H_3	$-H_1$	ϵ_{22}	μ_{33}	μ_{11}	$-J_2^e$	$-J_3^m$	J_1^m
TM	H_2	$-E_3$	E_1	μ_{22}	ϵ_{33}	ϵ_{11}	$-J_2^m$	J_3^e	$-J_1^e$

transformed equations, we obtain the following matrix-vector wave equation^{46–52}

$$\partial_3 \tilde{\mathbf{q}} = \tilde{\mathbf{A}} \tilde{\mathbf{q}} + \tilde{\mathbf{d}}, \tag{12}$$

with wave vector $\tilde{\mathbf{q}}(s_1, x_3, \omega)$ and source vector $\tilde{\mathbf{d}}(s_1, x_3, \omega)$ defined as

$$\tilde{\mathbf{q}} = \begin{pmatrix} \tilde{P} \\ \tilde{Q}_3 \end{pmatrix} \quad \text{and} \quad \tilde{\mathbf{d}} = \begin{pmatrix} \tilde{C}_3 \\ \tilde{B} + s_1 \tilde{C}_1 / \beta_1 \end{pmatrix} \tag{13}$$

and matrix $\tilde{\mathbf{A}}(s_1, x_3, \omega)$ defined as

$$\tilde{\mathbf{A}} = \begin{pmatrix} 0 & i\omega\beta_3 \\ i\omega s_3^2 / \beta_3 & 0 \end{pmatrix}, \tag{14}$$

with

$$s_3^2 = \alpha\beta_3 - \eta s_1^2, \quad \text{with} \quad \eta = \beta_3 / \beta_1. \tag{15}$$

Note that vector $\tilde{\mathbf{q}}$ defined in Eq. (13) contains the wave field quantities that are continuous at interfaces between layers with different medium parameters. Moreover, these quantities constitute the power flux density j in the x_3 -direction via $j = (1/2)\Re\{\tilde{P}^* \tilde{Q}_3\}$. In the matrix-vector notation, this can be written as

$$j = \frac{1}{4} \tilde{\mathbf{q}}^\dagger \mathbf{K} \tilde{\mathbf{q}}, \tag{16}$$

where \dagger denotes transposition and complex conjugation and where matrix \mathbf{K} is defined as

$$\mathbf{K} = \begin{pmatrix} 0 & 1 \\ 1 & 0 \end{pmatrix}. \tag{17}$$

The quantity s_3^2 defined in Eq. (15) is the square of the vertical phase slowness. Using Eqs. (7) and (8), it can be written as

$$s_3^2 = \frac{1}{c_0^2} h_x h_\beta - \eta_0 s_1^2, \tag{18}$$

with

$$c_0 = (\alpha_0 \beta_{3,0})^{-1/2} \quad \text{and} \quad \eta_0 = \beta_{3,0} / \beta_{1,0}. \tag{19}$$

Since h_x and h_β are complex-valued functions, s_3^2 is complex-valued as well. Defining $h_x = h_x^r + ih_x^i$ and $h_\beta = h_\beta^r + ih_\beta^i$, we may write

$$\Re(s_3^2) = \frac{1}{c_0^2} (h_x^r h_\beta^r - h_x^i h_\beta^i) - \eta_0 s_1^2, \tag{20}$$

$$\Im(s_3^2) = \frac{1}{c_0^2} (h_x^r h_\beta^i + h_x^i h_\beta^r). \tag{21}$$

For DPS media, with $h_x^r, h_\beta^r, h_x^i, h_\beta^i$ all positive (or zero), we have $\Im(s_3^2) \geq 0$. For this situation, Fig. 1(a) illustrates s_3^2 in

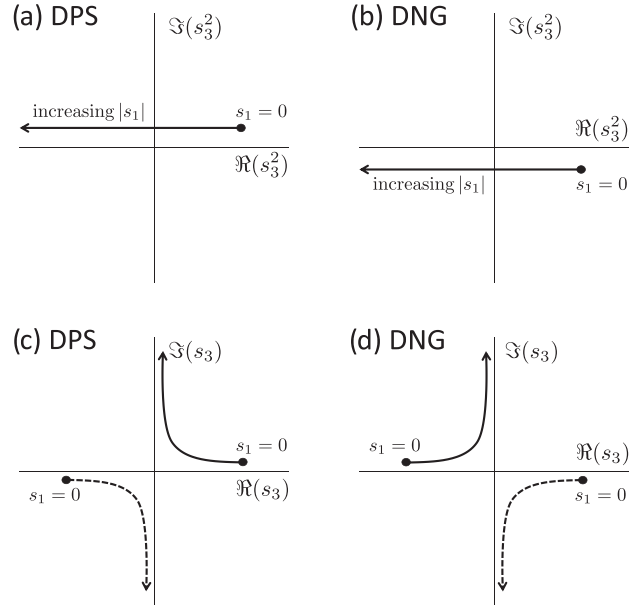


FIG. 1. Squared slowness s_3^2 in the complex plane for (a) DPS and (b) DNG medium. Slowness s_3 in the complex plane for (c) DPS and (d) DNG medium. The solid curves in (c) and (d) represent the proper square-roots of those in (a) and (b).

the complex plane for a fixed frequency ω and variable s_1 . For DNG media, with h_x^r, h_β^r both negative and h_x^i, h_β^i both positive, we have $\Im(s_3^2) < 0$. For this situation, s_3^2 is illustrated in the complex plane in Fig. 1(b).

C. Decomposition of matrix-vector wave equation

We reorganise the matrix-vector wave equation into an equation for downgoing and upgoing waves. The eigenvalue decomposition of matrix $\tilde{\mathbf{A}}(s_1, x_3, \omega)$ reads

$$\tilde{\mathbf{A}} = \tilde{\mathbf{L}} \tilde{\mathbf{\Lambda}} \tilde{\mathbf{L}}^{-1}, \tag{22}$$

with $\tilde{\mathbf{\Lambda}}(s_1, x_3, \omega)$, $\tilde{\mathbf{L}}(s_1, x_3, \omega)$, and $\{\tilde{\mathbf{L}}(s_1, x_3, \omega)\}^{-1}$ defined as

$$\tilde{\mathbf{A}} = \begin{pmatrix} i\omega s_3 & 0 \\ 0 & -i\omega s_3 \end{pmatrix}, \tag{23}$$

$$\tilde{\mathbf{L}} = \begin{pmatrix} 1 & 1 \\ s_3/\beta_3 & -s_3/\beta_3 \end{pmatrix}, \tag{24}$$

$$\tilde{\mathbf{L}}^{-1} = \frac{1}{2} \begin{pmatrix} 1 & \beta_3/s_3 \\ 1 & -\beta_3/s_3 \end{pmatrix}. \tag{25}$$

The vertical phase slowness s_3 is defined as the square-root of s_3^2 , i.e.,

$$s_3 = \pm \sqrt{\frac{1}{c_0^2} h_x h_\beta - \eta_0 s_1^2}. \tag{26}$$

It is illustrated in Figs. 1(c) and 1(d) for DPS and DNG media, respectively. In both cases, there are two square-roots indicated

by the two curves in these figures. In Sec. II D, we discuss how to choose the proper square-roots.

We introduce a decomposed field vector $\tilde{\mathbf{p}}$ and a decomposed source vector $\tilde{\mathbf{s}}$ via

$$\tilde{\mathbf{q}} = \tilde{\mathbf{L}}\tilde{\mathbf{p}}, \tag{27}$$

$$\tilde{\mathbf{d}} = \tilde{\mathbf{L}}\tilde{\mathbf{s}}, \tag{28}$$

with

$$\tilde{\mathbf{p}} = \begin{pmatrix} \tilde{P}^+ \\ \tilde{P}^- \end{pmatrix}, \quad \tilde{\mathbf{s}} = \begin{pmatrix} \tilde{S}^+ \\ \tilde{S}^- \end{pmatrix}. \tag{29}$$

Substitution of Eqs. (22), (27), and (28) into the matrix-vector wave Eq. (12) yields

$$\partial_3 \tilde{\mathbf{p}} = (\tilde{\mathbf{A}} - \tilde{\mathbf{L}}^{-1} \partial_3 \tilde{\mathbf{L}}) \tilde{\mathbf{p}} + \tilde{\mathbf{s}}. \tag{30}$$

This is a coupled system of equations for the wave field components \tilde{P}^+ and \tilde{P}^- , respectively. According to Eqs. (13), (24), (27), and (29), we have

$$\tilde{P} = \tilde{P}^+ + \tilde{P}^-, \tag{31}$$

hence, the wave field components \tilde{P}^+ and \tilde{P}^- have the same physical dimension as the field quantity \tilde{P} . Therefore, we speak of field-normalised decomposition (opposed to flux-normalized decomposition).

From the theory for lossless DPS media, it is known that the components \tilde{P}^+ and \tilde{P}^- represent downgoing and upgoing wave fields, respectively.^{48–51,53} This still holds true for DPS and DNG media with or without losses, provided the proper choices are made for the sign of the vertical phase slowness s_3 . This is discussed in Sec. II D.

D. Phase slowness

We can express the power flux density j in the x_3 -direction in terms of downgoing and upgoing wave fields by substituting $\tilde{\mathbf{q}} = \tilde{\mathbf{L}}\tilde{\mathbf{p}}$ into Eq. (16). Using Eqs. (17) and (24), we thus obtain

$$\begin{aligned} j &= \frac{1}{4} \tilde{\mathbf{q}}^\dagger \mathbf{K} \tilde{\mathbf{q}} = \frac{1}{4} \tilde{\mathbf{p}}^\dagger \tilde{\mathbf{L}}^\dagger \mathbf{K} \tilde{\mathbf{L}} \tilde{\mathbf{p}} \\ &= \frac{1}{2} \Re(s_3/\beta_3) (|\tilde{P}^+|^2 - |\tilde{P}^-|^2) + \Im(s_3/\beta_3) \Im((\tilde{P}^+)^* \tilde{P}^-). \end{aligned} \tag{32}$$

For the discussion on the sign of the vertical phase slowness s_3 , consider an independent downgoing wave field \tilde{P}^+ in a homogeneous medium. For this situation, the power flux density can be written as

$$j = \frac{1}{2} \Re(s_3/\beta_3) |\tilde{P}^+|^2 = \frac{h_\beta^r \Re(s_3) + h_\beta^i \Im(s_3)}{2\beta_{3,0} |h_\beta|^2} |\tilde{P}^+|^2, \tag{33}$$

where we used Eq. (8) to express β_3 in terms of the positive quantity $\beta_{3,0}$ and $h_\beta = h_\beta^r + ih_\beta^i$. We now determine the

signs of $\Re(s_3)$ and $\Im(s_3)$ such that \tilde{P}^+ has a positive power flux density in the positive x_3 -direction.²⁴ For DPS media, with h_β^r and h_β^i both positive, we find that this condition is fulfilled when $\Re(s_3) > 0$ and $\Im(s_3) > 0$. Hence, the solid curve in Fig. 1(c) represents the proper square-root of s_3^2 . We write this square-root as

$$s_3 = +\sqrt{\frac{1}{c_0^2} h_\alpha h_\beta - \eta_0 s_1^2}, \tag{34}$$

with the + sign in front of the square-root denoting that $\Re(s_3) > 0$. For DNG media, with h_β^r negative and h_β^i positive, we find that j is positive when $\Re(s_3) < 0$ and $\Im(s_3) > 0$. Hence, for this situation, the solid curve in Fig. 1(d) represents the proper square-root of s_3^2 . We write this square-root as

$$s_3 = -\sqrt{\frac{1}{c_0^2} h_\alpha h_\beta - \eta_0 s_1^2}, \tag{35}$$

with the – sign in front of the square-root denoting that $\Re(s_3) < 0$. Equations (34) and (35) express the fact that the (real part of the) vertical phase slowness is positive for DPS media and negative for DNG media. Given these square-roots, we find in the same way that j is negative for an independent upgoing wave field \tilde{P}^- in a homogeneous medium.

Figure 2 shows s_3^2 and s_3 in the complex plane for the limiting situation of vanishing losses, i.e., vanishing imaginary parts of the medium parameters. Note that the real and imaginary branches of s_3 correspond to propagating and evanescent waves, respectively.

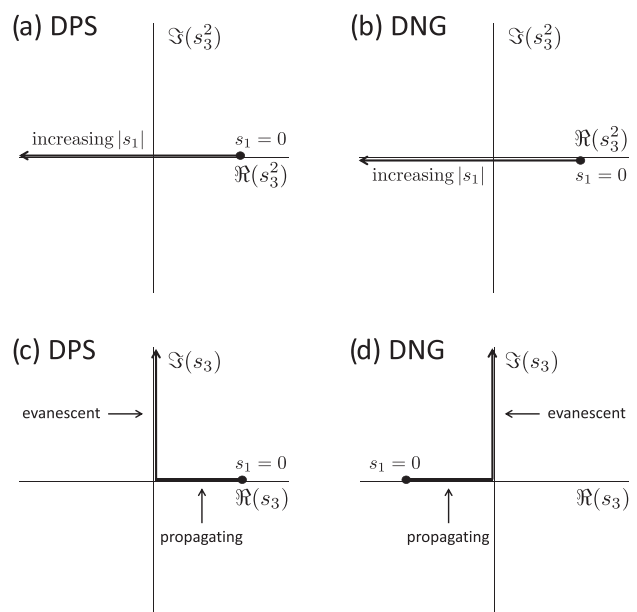


FIG. 2. As Fig. 1, for the limiting case of vanishing loss parameters. The curves in (c) and (d) are the proper square-roots of those in (a) and (b).

E. Group slowness

Despite the fact that the vertical phase slowness in a DNG medium is negative, the vertical group slowness should be positive. This restricts the choice of models for the functions $h_\alpha(\omega)$ and $h_\beta(\omega)$. We define the vertical group slowness as

$$s_3^{gr} = \Re\left(\frac{\partial(\omega s_3)}{\partial\omega}\right). \tag{36}$$

Substituting Eq. (35), taking for convenience $h_\alpha(\omega) = h_\beta(\omega) = h(\omega)$, we obtain

$$s_3^{gr} = \Re\left(\frac{h\left(h + \omega \frac{\partial h}{\partial\omega}\right) - \eta_0 c_0^2 s_1^2}{c_0^2 s_3}\right). \tag{37}$$

We analyse this expression for the Drude model of Eqs. (9) and (10), with $\omega_\alpha = \omega_\beta = \omega_0$ and $\Gamma_\alpha = \Gamma_\beta = \Gamma$, hence

$$h(\omega) = 1 - \frac{\omega_0^2}{\omega(\omega + i\Gamma)} \tag{38}$$

and

$$h + \omega \partial h / \partial \omega = 1 + \frac{\omega_0^2}{(\omega + i\Gamma)^2}. \tag{39}$$

The condition for a DNG medium, $\Re(h) < 0$, requires $\omega^2 < \omega_0^2 - \Gamma^2$.

We evaluate the sign of s_3^{gr} for two special situations. First, we consider vertically propagating waves, i.e., $s_1 = 0$. From Eq. (35), we find $s_3 = h/c_0$ for $\omega^2 < \omega_0^2 - \Gamma^2$. Using this in Eq. (37), we obtain²⁶

$$s_3^{gr} = \frac{\Re(h + \omega \partial h / \partial \omega)}{c_0} = \frac{1}{c_0} \Re\left(1 + \frac{\omega_0^2}{(\omega + i\Gamma)^2}\right). \tag{40}$$

Assuming small Γ (a sufficient condition is $\Gamma < \omega$), we find indeed that the vertical group slowness s_3^{gr} is positive.

Next, we consider non-zero s_1 and analyse Eq. (37) for the limit $\Gamma \rightarrow 0$. From Eqs. (38) and (39), we find $h = 1 - \omega_0^2/\omega^2$ and $h(h + \omega \partial h / \partial \omega) = 1 - \omega_0^4/\omega^4$. Using this in Eq. (37), we obtain

$$s_3^{gr} = \frac{\eta_0 c_0^2 s_1^2 + \omega_0^4/\omega^4 - 1}{c_0^2 \sqrt{(\omega_0^2/\omega^2 - 1)^2/c_0^2 - \eta_0 s_1^2}}. \tag{41}$$

For $\omega < \omega_0$, the nominator is positive for all s_1 . For propagating waves, the denominator is real-valued and positive as well, hence s_3^{gr} is positive for this situation.

III. REPRESENTATIONS FOR THE MARCHENKO METHOD

A. Propagation invariants for DPS and DNG media

We consider a medium configuration consisting of a homogeneous DPS upper half-space $x_3 \leq x_{3,0}$ and a

horizontally layered lower half-space $x_3 > x_{3,0}$, which may consist of an arbitrary mix of DPS and DNG layers. The effective medium parameters in this configuration are $\alpha(x_3, \omega)$ and $\beta_i(x_3, \omega)$. These parameters may vary continuously as a function of x_3 within each layer and jump by a finite amount at layer interfaces. We assume that the losses are small, and for the derivation of the Marchenko method, we ignore the imaginary parts of $\alpha(x_3, \omega)$ and $\beta_i(x_3, \omega)$ (however, in the numerical example in Sec. V, we model the input data with complex-valued medium parameters). Assuming that the sources are restricted to the upper half-space $x_3 \leq x_{3,0}$, the wave field inside the layers is governed by wave Eq. (12) with $\tilde{\mathbf{d}} = 0$. Moreover, $\tilde{\mathbf{q}}$ is continuous at layer interfaces. We derive propagation invariants,^{54–57} which we will use for the derivation of the representations for the Marchenko method in Sec. III B. We consider two independent wave vectors $\tilde{\mathbf{q}}_A$ and $\tilde{\mathbf{q}}_B$ and will show that $\tilde{\mathbf{q}}_A^t \mathbf{N} \tilde{\mathbf{q}}_B$ and $\tilde{\mathbf{q}}_A^t \mathbf{K} \tilde{\mathbf{q}}_B$ are propagation invariants (i.e., that they are independent of the coordinate x_3 for $x_3 > x_{3,0}$). Here superscript t denotes transposition and matrix \mathbf{N} is defined as

$$\mathbf{N} = \begin{pmatrix} 0 & 1 \\ -1 & 0 \end{pmatrix}. \tag{42}$$

Obviously, the quantities $\tilde{\mathbf{q}}_A^t \mathbf{N} \tilde{\mathbf{q}}_B$ and $\tilde{\mathbf{q}}_A^t \mathbf{K} \tilde{\mathbf{q}}_B$ are continuous at layer interfaces. Hence, to show that these quantities are propagation invariants for the layered medium, it suffices to show that they are propagation invariants inside a layer. Evaluating $\partial_3\{\tilde{\mathbf{q}}_A^t \mathbf{N} \tilde{\mathbf{q}}_B\}$ and $\partial_3\{\tilde{\mathbf{q}}_A^t \mathbf{K} \tilde{\mathbf{q}}_B\}$, using Eq. (12) with $\tilde{\mathbf{d}} = 0$, we obtain

$$\partial_3\{\tilde{\mathbf{q}}_A^t \mathbf{N} \tilde{\mathbf{q}}_B\} = \tilde{\mathbf{q}}_A^t \tilde{\mathbf{A}}^t \mathbf{N} \tilde{\mathbf{q}}_B + \tilde{\mathbf{q}}_A^t \mathbf{N} \tilde{\mathbf{A}} \tilde{\mathbf{q}}_B, \tag{43}$$

$$\partial_3\{\tilde{\mathbf{q}}_A^t \mathbf{K} \tilde{\mathbf{q}}_B\} = \tilde{\mathbf{q}}_A^t \tilde{\mathbf{A}}^t \mathbf{K} \tilde{\mathbf{q}}_B + \tilde{\mathbf{q}}_A^t \mathbf{K} \tilde{\mathbf{A}} \tilde{\mathbf{q}}_B. \tag{44}$$

Matrix $\tilde{\mathbf{A}}$, defined in Eq. (14), obeys for real-valued medium parameters the following symmetry relations:

$$\tilde{\mathbf{A}}^t \mathbf{N} = -\mathbf{N} \tilde{\mathbf{A}}, \tag{45}$$

$$\tilde{\mathbf{A}}^t \mathbf{K} = -\mathbf{K} \tilde{\mathbf{A}}. \tag{46}$$

Hence, the right-hand sides of Eqs. (43) and (44) are equal to zero, which confirms that $\tilde{\mathbf{q}}_A^t \mathbf{N} \tilde{\mathbf{q}}_B$ and $\tilde{\mathbf{q}}_A^t \mathbf{K} \tilde{\mathbf{q}}_B$ are propagation invariants.

Next, we derive propagation invariants for decomposed wave fields. Consider two independent decomposed wave vectors $\tilde{\mathbf{p}}_A$ and $\tilde{\mathbf{p}}_B$, which are related to $\tilde{\mathbf{q}}_A$ and $\tilde{\mathbf{q}}_B$, respectively, via Eq. (27). We obtain propagation invariants for these decomposed wave vectors by substituting $\tilde{\mathbf{q}}_A = \tilde{\mathbf{L}} \tilde{\mathbf{p}}_A$ and $\tilde{\mathbf{q}}_B = \tilde{\mathbf{L}} \tilde{\mathbf{p}}_B$ into the propagation invariants $\tilde{\mathbf{q}}_A^t \mathbf{N} \tilde{\mathbf{q}}_B$ and $\tilde{\mathbf{q}}_A^t \mathbf{K} \tilde{\mathbf{q}}_B$. Using Eqs. (17), (24), and (42), we obtain

$$\tilde{\mathbf{q}}_A^t \mathbf{N} \tilde{\mathbf{q}}_B = \tilde{\mathbf{p}}_A^t \tilde{\mathbf{L}}^t \mathbf{N} \tilde{\mathbf{L}} \tilde{\mathbf{p}}_B = -2(s_3/\beta_3) \tilde{\mathbf{p}}_A^t \mathbf{N} \tilde{\mathbf{p}}_B \tag{47}$$

and

$$\begin{aligned} \tilde{\mathbf{q}}_A^\dagger \mathbf{K} \tilde{\mathbf{q}}_B &= \tilde{\mathbf{p}}_A^\dagger \tilde{\mathbf{L}}^\dagger \mathbf{K} \tilde{\mathbf{L}} \tilde{\mathbf{p}}_B \\ &= 2\tilde{\mathbf{p}}_A^\dagger [\Re(s_3/\beta_3)\mathbf{J} - i\Im(s_3/\beta_3)\mathbf{N}] \tilde{\mathbf{p}}_B, \end{aligned} \quad (48)$$

with

$$\mathbf{J} = \begin{pmatrix} 1 & 0 \\ 0 & -1 \end{pmatrix}. \quad (49)$$

From Eqs. (29), (42), and (47), we obtain the propagation invariant

$$(s_3/\beta_3)(\tilde{P}_A^+ \tilde{P}_B^- - \tilde{P}_A^- \tilde{P}_B^+). \quad (50)$$

From Eqs. (29), (48), and (49) we obtain for propagating waves (i.e., for real-valued s_3) the propagation invariant

$$(s_3/\beta_3)[(\tilde{P}_A^+)^* \tilde{P}_B^+ - (\tilde{P}_A^-)^* \tilde{P}_B^-]. \quad (51)$$

B. Representations

We use the propagation invariants of Eqs. (50) and (51) to derive representations for the Marchenko method. We introduce decomposed focusing functions [Fig. 3(a)] and Green's functions [Fig. 3(b)] and derive relations between them using Eqs. (50) and (51), with \tilde{P}_A^\pm and \tilde{P}_B^\pm replaced by the focusing functions and Green's functions, respectively.^{14,15}

First we discuss the Green's functions. For the source quantities in Eq. (13), we take $\tilde{B}(s_1, x_3, \omega) = \delta(x_3 - x_{3,0}^\epsilon)$ and $\tilde{C}_i(s_1, x_3, \omega) = 0$, where $x_{3,0}^\epsilon = x_{3,0} - \epsilon$, with ϵ a vanishing positive constant, so that the source of the Green's function is located in the homogeneous upper half-space, just above $x_{3,0}$ [Fig. 3(b)]. For the wave field \tilde{P} in Eq. (13), we take $\tilde{P} = \tilde{G}(s_1, x_3, x_{3,0}^\epsilon, \omega)$, with $x_{3,0}^\epsilon$ and x_3 denoting the source and receiver coordinates of the Green's function. We decompose the Green's function at the receiver position x_3 into downgoing and upgoing components $\tilde{P}^+ = \tilde{G}^+(s_1, x_3, x_{3,0}^\epsilon, \omega)$ and $\tilde{P}^- = \tilde{G}^-(s_1, x_3, x_{3,0}^\epsilon, \omega)$, respectively. Analogous to Eq. (31), these components are related to the total Green's function via

$$\tilde{G} = \tilde{G}^+ + \tilde{G}^-. \quad (52)$$

Furthermore, according to equations (13), (25), (28) and (29), the decomposed Green's sources are related to the total Green's source $\tilde{B}(s_1, x_3, \omega) = \delta(x_3 - x_{3,0}^\epsilon)$ via

$$\tilde{S}^\pm(s_1, x_3, \omega) = \pm(\beta_3/2s_3)\delta(x_3 - x_{3,0}^\epsilon). \quad (53)$$

The source \tilde{S}^- radiates upgoing waves into the homogeneous half-space above $x_{3,0}^\epsilon$, which will not return into the layered medium and will not, therefore, be considered further. The source \tilde{S}^+ radiates downgoing waves into the medium below $x_{3,0}^\epsilon$. Due to propagation and scattering in the layered medium, the field at any depth $x_3 \geq x_{3,0}^\epsilon$ consists of the downgoing and upgoing components $\tilde{G}^+(s_1, x_3, x_{3,0}^\epsilon, \omega)$

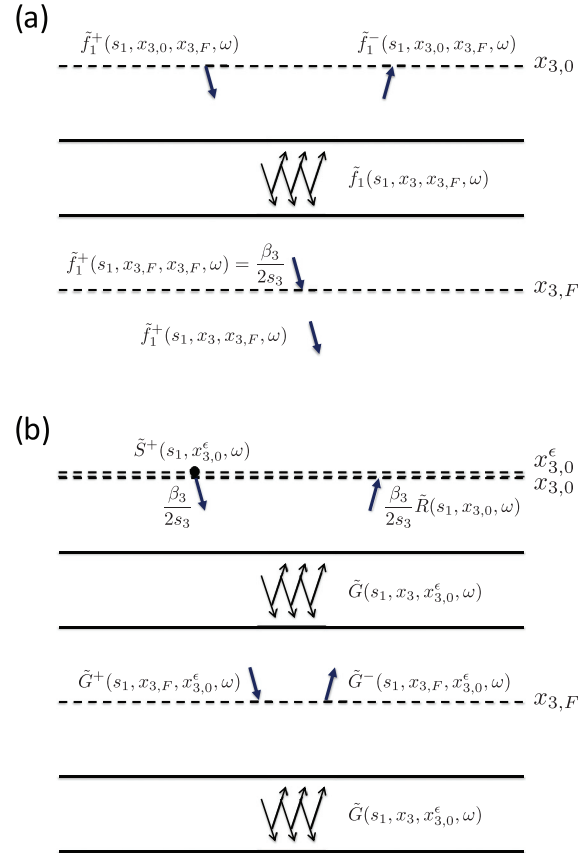


FIG. 3. (a) The focusing function $\tilde{f}_1 = \tilde{f}_1^+ + \tilde{f}_1^-$, defined in a truncated version of the actual medium. (b) The Green's function $\tilde{G} = \tilde{G}^+ + \tilde{G}^-$, defined in the actual medium.

and $\tilde{G}^-(s_1, x_3, x_{3,0}^\epsilon, \omega)$. At $x_3 = x_{3,0}$, i.e., at a vanishing distance ϵ below the source, the downgoing component reads

$$\begin{aligned} \tilde{G}^+(s_1, x_{3,0}, x_{3,0}^\epsilon, \omega) &= (\beta_3/2s_3) \lim_{\epsilon \rightarrow 0} \exp\{i\omega s_3 \epsilon\} \\ &= \frac{\beta_3(x_{3,0}, \omega)}{2s_3(s_1, x_{3,0}, \omega)}. \end{aligned} \quad (54)$$

This follows from Eqs. (23), (29), (30), and (53), taking into account that the medium between $x_{3,0}^\epsilon$ and $x_{3,0}$ is homogeneous. At the same depth level ($x_3 = x_{3,0}$), we relate the upgoing component to the reflection response $\tilde{R}(s_1, x_{3,0}, \omega)$ of the layered medium, via

$$\tilde{G}^-(s_1, x_{3,0}, x_{3,0}^\epsilon, \omega) = \frac{\beta_3(x_{3,0}, \omega)\tilde{R}(s_1, x_{3,0}, \omega)}{2s_3(s_1, x_{3,0}, \omega)}, \quad (55)$$

where the factor $\beta_3/2s_3$ is introduced to compensate for the source properties expressed by Eq. (53). The decomposed Green's functions \tilde{G}^+ and \tilde{G}^- will be substituted for \tilde{P}_B^+ and \tilde{P}_B^- in the propagation invariants of Eqs. (50) and (51). Table II shows these functions at depth level $x_3 = x_{3,0}$ (just below the source) and at an arbitrary depth level $x_3 = x_{3,F}$ (with $x_{3,F} > x_{3,0}$) inside the layered medium. Note that for convenience, we dropped the superscript ϵ from $x_{3,0}^\epsilon$.

TABLE II. Quantities used in the propagation invariants of Eqs. (50) and (51).

	$\tilde{P}_A^+(s_1, x_3, \omega)$	$\tilde{P}_A^-(s_1, x_3, \omega)$	$\tilde{P}_B^+(s_1, x_3, \omega)$	$\tilde{P}_B^-(s_1, x_3, \omega)$
$x_3 = x_{3,0}$	$\tilde{f}_1^+(s_1, x_{3,0}, x_{3,F}, \omega)$	$\tilde{f}_1^-(s_1, x_{3,0}, x_{3,F}, \omega)$	$\beta_3(x_{3,0}, \omega)/2s_3(s_1, x_{3,0}, \omega)$	$\beta_3(x_{3,0}, \omega)\tilde{R}(s_1, x_{3,0}, \omega)/2s_3(s_1, x_{3,0}, \omega)$
$x_3 = x_{3,F}$	$\beta_3(x_{3,F}, \omega)/2s_3(s_1, x_{3,F}, \omega)$	0	$\tilde{G}^+(s_1, x_{3,F}, x_{3,0}, \omega)$	$\tilde{G}^-(s_1, x_{3,F}, x_{3,0}, \omega)$

Next we discuss the focusing functions.⁵⁸ We define these functions in a truncated version of the actual medium [Fig. 3(a)]. This truncated medium is taken identical to the actual medium above $x_3 = x_{3,F}$ and homogeneous below this depth level. We call $x_{3,F}$ the focal depth. Analogous to Eq. (52), we define the focusing function $\tilde{f}_1(s_1, x_3, x_{3,F}, \omega)$ as a superposition of downgoing and upgoing components $\tilde{f}_1^+(s_1, x_3, x_{3,F}, \omega)$ and $\tilde{f}_1^-(s_1, x_3, x_{3,F}, \omega)$, respectively, according to

$$\tilde{f}_1 = \tilde{f}_1^+ + \tilde{f}_1^- \tag{56}$$

The downgoing focusing function $\tilde{f}_1^+(s_1, x_{3,0}, x_{3,F}, \omega)$ is incident to the truncated layered medium from the upper boundary $x_{3,0}$ and is designed such that $\tilde{f}_1^+(s_1, x_3, x_{3,F}, \omega)$ focuses at the focal depth $x_3 = x_{3,F}$. Inside the medium, propagation and scattering takes place and the upgoing focusing function $\tilde{f}_1^-(s_1, x_3, x_{3,F}, \omega)$ eventually reaches the upper boundary $x_3 = x_{3,0}$. Below the focal depth $x_{3,F}$, the focusing function continues propagating downward into the homogeneous lower half-space of the truncated medium. We define $\tilde{T}(s_1, x_{3,F}, x_{3,0}, \omega)$ as the transmission response of the truncated medium between $x_{3,0}$ and $x_{3,F}$. Hence, the propagation of the focusing function from $x_{3,0}$ to $x_{3,F}$ is described by

$$\tilde{f}_1^+(s_1, x_{3,F}, x_{3,F}, \omega) = \tilde{T}(s_1, x_{3,F}, x_{3,0}, \omega)\tilde{f}_1^+(s_1, x_{3,0}, x_{3,F}, \omega) \tag{57}$$

The left-hand side describes the focused field at $x_{3,F}$. We could define this as $\tilde{f}_1^+(s_1, x_{3,F}, x_{3,F}, \omega) = 1$ (with the inverse Fourier transform of 1 being a temporal delta function). However, in analogy with the Green’s function at the source depth in Eq. (54), we define the focused field at the focal depth as

$$\tilde{f}_1^+(s_1, x_{3,F}, x_{3,F}, \omega) = \frac{\beta_3(x_{3,F}, \omega)}{2s_3(s_1, x_{3,F}, \omega)} \tag{58}$$

From Eqs. (57) and (58), it follows that the downgoing focusing function $\tilde{f}_1^+(s_1, x_3, x_{3,F}, \omega)$ for $x_3 = x_{3,0}$ is related to the transmission response of the truncated medium via

$$\tilde{f}_1^+(s_1, x_{3,0}, x_{3,F}, \omega) = \frac{\beta_3(x_{3,F}, \omega)}{2s_3(s_1, x_{3,F}, \omega)\tilde{T}(s_1, x_{3,F}, x_{3,0}, \omega)} \tag{59}$$

Since the truncated medium is homogeneous below the focal depth, there is no upgoing field at the focal depth, hence

$$\tilde{f}_1^-(s_1, x_{3,F}, x_{3,F}, \omega) = 0 \tag{60}$$

The decomposed focusing functions \tilde{f}_1^+ and \tilde{f}_1^- will be substituted for \tilde{P}_A^+ and \tilde{P}_A^- in the propagation invariants of Eqs. (50) and (51). Table II shows these functions at depth levels $x_3 = x_{3,0}$ and $x_3 = x_{3,F}$. An underlying assumption for the propagation invariants is that the fields \tilde{P}_A^\pm and \tilde{P}_B^\pm are defined in the same source-free medium. This condition is fulfilled in the region between $x_{3,0}$ and $x_{3,F}$. Substituting the quantities of Table II into the propagation invariant of Eq. (50) and equating the results for $x_{3,0}$ and $x_{3,F}$ yields

$$\begin{aligned} \tilde{G}^-(s_1, x_{3,F}, x_{3,0}, \omega) + \tilde{f}_1^-(s_1, x_{3,0}, x_{3,F}, \omega) \\ = \tilde{R}(s_1, x_{3,0}, \omega)\tilde{f}_1^+(s_1, x_{3,0}, x_{3,F}, \omega) \end{aligned} \tag{61}$$

In a similar way, we obtain from the propagation invariant of Eq. (51) for propagating waves

$$\begin{aligned} \tilde{G}^+(s_1, x_{3,F}, x_{3,0}, \omega) - \{\tilde{f}_1^+(s_1, x_{3,0}, x_{3,F}, \omega)\}^* \\ = -\tilde{R}(s_1, x_{3,0}, \omega)\{\tilde{f}_1^-(s_1, x_{3,0}, x_{3,F}, \omega)\}^* \end{aligned} \tag{62}$$

These representations express the downgoing and upgoing components of the Green’s function at an arbitrarily chosen depth level $x_3 = x_{3,F}$ in terms of the reflection response at the surface $x_3 = x_{3,0}$ and decomposed focusing functions. These representations hold for a layered medium consisting of an arbitrary mix of DPS and DNG layers. The reflection response $\tilde{R}(s_1, x_{3,0}, \omega)$ can be obtained from measurements at the surface $x_{3,0}$. According to Eq. (59), the focusing function $\tilde{f}_1^+(s_1, x_{3,0}, x_{3,F}, \omega)$ could in principle be obtained from the transmission response of the truncated medium. However, this would require detailed knowledge of the medium between $x_{3,0}$ and $x_{3,F}$. In Sec. IV, we discuss the Marchenko method, which enables retrieving the focusing functions from the reflection response at the surface and a background model of the medium.

IV. THE MARCHENKO METHOD

We start by transforming the representations of Eqs. (61) and (62) to the time domain. Analogous to Eq. (3), we define the following inverse Fourier transform:

$$u(s_1, x_3, \tau) = \frac{1}{\pi} \Re \int_0^\infty \tilde{u}(s_1, x_3, \omega) \exp(-i\omega\tau) d\omega \tag{63}$$

where τ is the so-called intercept time.⁵⁹ Applying this inverse transform to Eqs. (61) and (62), we obtain

$$G^-(s_1, x_{3,F}, x_{3,0}, \tau) + f_1^-(s_1, x_{3,0}, x_{3,F}, \tau) = \int_{-\infty}^{\tau} R(s_1, x_{3,0}, \tau - \tau') f_1^+(s_1, x_{3,0}, x_{3,F}, \tau') d\tau' \quad (64)$$

and

$$G^+(s_1, x_{3,F}, x_{3,0}, \tau) - f_1^+(s_1, x_{3,0}, x_{3,F}, -\tau) = - \int_{-\infty}^{\tau} R(s_1, x_{3,0}, \tau - \tau') f_1^-(s_1, x_{3,0}, x_{3,F}, -\tau') d\tau'. \quad (65)$$

For the derivation of the Marchenko method, we need time windows that suppress the Green's functions on the left-hand sides of the representations in Eqs. (64) and (65) so that we are left with two equations for the two focusing functions. First, we briefly review these windows for the situation of a layered medium consisting of DPS layers only. Figure 4 shows an example of the functions on the left-hand sides of Eqs. (64) and (65) for such a medium. Note that these functions (represented by the solid lines) have been convolved with a symmetric band-limited wavelet. For convenience, they have also been multiplied by a factor $2s_3/\beta_3$ to compensate for the source properties defined in Eq. (53). Figures 4(a) and 4(b) show the functions on the left-hand side of Eq. (65). The direct arrival of the downgoing Green's function $G^+(s_1, x_{3,F}, x_{3,0}, \tau)$ in Fig. 4(a) coincides with the time-reversed direct arrival of the focusing function $f_1^+(s_1, x_{3,0}, x_{3,F}, \tau)$ in Fig. 4(b). For this focusing function, we write

$$f_1^+(s_1, x_{3,0}, x_{3,F}, \tau) = f_{1,d}^+(s_1, x_{3,0}, x_{3,F}, \tau) + M^+(s_1, x_{3,0}, x_{3,F}, \tau), \quad (66)$$

where $f_{1,d}^+$ is the direct arrival and M^+ a coda, following the direct arrival [in Fig. 4(b), this coda is time-reversed and consists of a single event only, but more generally it consists of multiple events]. We define a time window $w(s_1, \tau) = \theta(\tau_d(s_1) - \tau_\epsilon - \tau)$, where $\theta(\tau)$ is the Heaviside step function, $\tau_d(s_1)$ the traveltime of the direct arrival of the downgoing Green's function, and τ_ϵ is half the duration of the symmetric wavelet. This window is indicated by the dashed lines in Fig. 4. It suppresses the downgoing Green's function in Fig. 4(a) and the time-reversed direct arrival of the focusing function in Fig. 4(b). It passes the time-reversed coda $M^+(s_1, x_{3,0}, x_{3,F}, -\tau)$ in Fig. 4(b). Figures 4(c) and 4(d) show the functions on the left-hand side of Eq. (64). Since the first arrival of the upgoing Green's function $G^-(s_1, x_{3,F}, x_{3,0}, \tau)$ arrives later than that of the downgoing Green's function, the time window $w(s_1, \tau)$ suppresses the upgoing Green's function in Fig. 4(c). It passes the focusing function $f_1^-(s_1, x_{3,0}, x_{3,F}, \tau)$ in Fig. 4(d). Applying the window to both sides of Eqs. (64) and (65), the windowed equations can be solved for $f_1^-(s_1, x_{3,0}, x_{3,F}, \tau)$ and $M^+(s_1, x_{3,0}, x_{3,F}, \tau)$, after which the Green's functions follow from the unwinded equations.^{14,15}

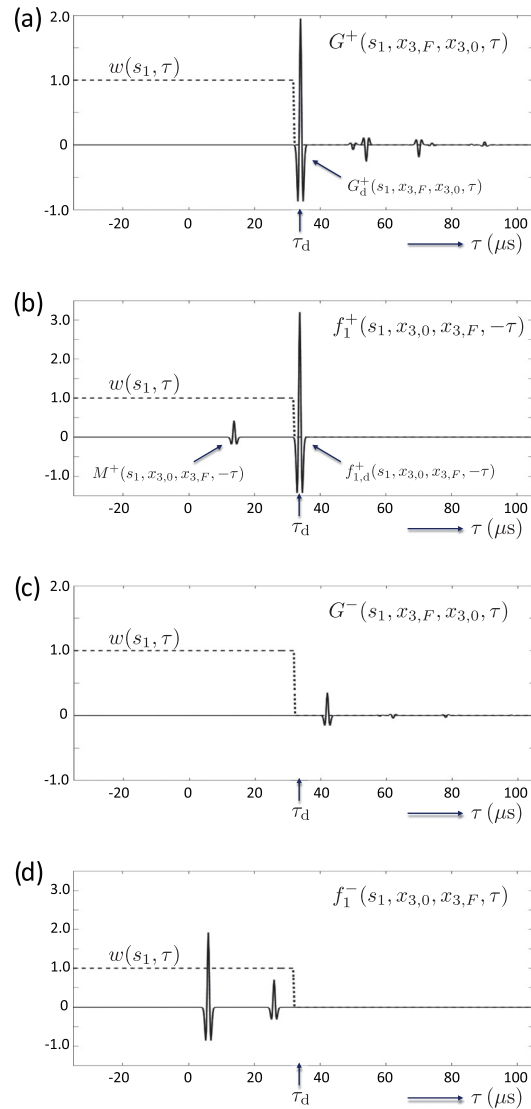


FIG. 4. The Green's functions and focusing functions on the left-hand sides of Eqs. (64) and (65), for the situation of a layered medium consisting of DPS layers only. The time window $w(s_1, \tau)$, indicated by the dashed lines, is the same for all functions.

Next, we discuss the time windows for the situation of a layered medium consisting of a mix of DPS and DNG layers. Figures 5(a) and 5(b) show an example of the functions on the left-hand side of Eq. (65) (again convolved with a symmetric band-limited wavelet and multiplied by a factor $2s_3/\beta_3$). Due to the highly dispersive character of the DNG layers, these functions are very different from their counterparts in Figs. 4(a) and 4(b). Nevertheless, for the focusing function $f_1^+(s_1, x_{3,0}, x_{3,F}, \tau)$, we can again distinguish between a direct arrival $f_{1,d}^+$ and a coda M^+ ; see Fig. 5(b) and Eq. (66). We define a time window

$$w^+(s_1, \tau) = \theta(\tau_{on}^+(s_1) - \tau), \quad (67)$$

where $\tau_{on}^+(s_1)$ is the traveltime of the onset of the downgoing Green's function. This window is indicated by the dashed lines in Figs. 5(a) and 5(b). This window suppresses the downgoing Green's function in Fig. 5(a) and the time-reversed direct

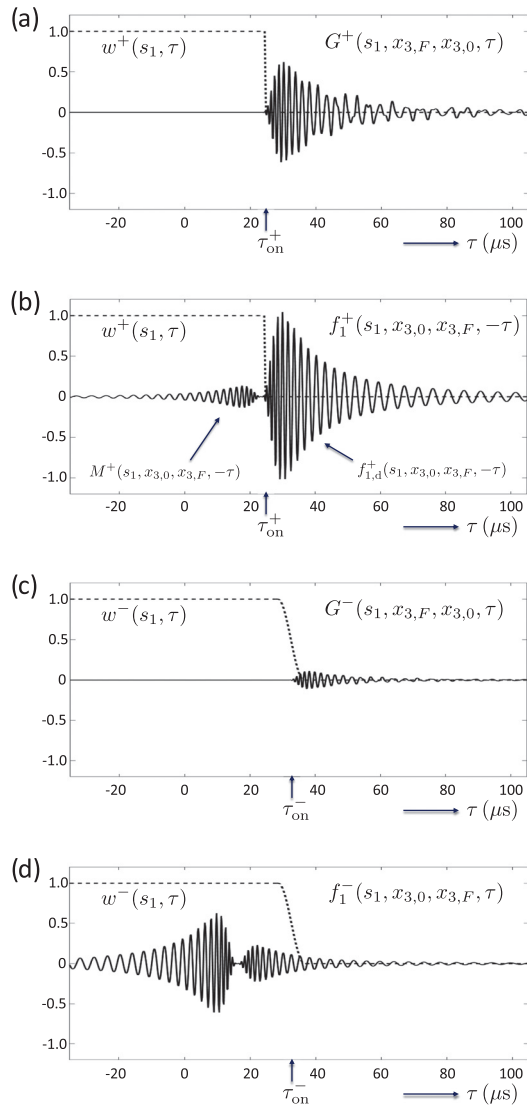


FIG. 5. As Fig. 4, but for the situation of a layered medium consisting of DPS and DNG layers. Note the different time windows $w^+(s_1, \tau)$ and $w^-(s_1, \tau)$, indicated by the dashed lines.

arrival of the focusing function in Fig. 5(b); it passes the time-reversed coda $M^+(s_1, x_{3,0}, x_{3,F}, -\tau)$ in Fig. 5(b). Figures 5(c) and 5(d) show the functions on the left-hand side of Eq. (64). The onset time $\tau_{\text{on}}^-(s_1)$ of the upgoing Green's function in Fig. 5(c) is larger than that of the downgoing Green's function. Note, however, that the dispersive tail of $f_1^-(s_1, x_{3,0}, x_{3,F}, \tau)$ in Fig. 5(d) exceeds not only the onset time of the downgoing Green's function but also that of the upgoing Green's function. Hence, the upgoing Green's function in Fig. 5(c) and the focusing function in Fig. 5(d) cannot be uniquely separated by a time window. We define a time window

$$w^-(s_1, \tau) = \theta_{\text{tap}}(\tau_{\text{on}}^-(s_1) - \tau), \quad (68)$$

where $\theta_{\text{tap}}(\tau)$ is a tapered step function. It is indicated by the dashed lines in Figs. 5(c) and 5(d). The taper should be chosen such that this window suppresses the upgoing Green's function in Fig. 5(c) as well as possible and leaves the focusing function $f_1^-(s_1, x_{3,0}, x_{3,F}, \tau)$ in Fig. 5(d) intact as much as

possible. It is unavoidable that this approach leads to approximations, particularly in the situation of thin layers.

Assuming a proper window function $w^-(s_1, \tau)$ can be found, the application of this window to both sides of Eq. (64), and window $w^+(s_1, \tau)$ to both sides of Eq. (65), yields the following system of coupled Marchenko equations for $f_1^-(s_1, x_{3,0}, x_{3,F}, \tau)$ and $M^+(s_1, x_{3,0}, x_{3,F}, \tau)$:

$$f_1^-(s_1, x_{3,0}, x_{3,F}, \tau) = w^-(s_1, \tau) \int_{-\infty}^{\tau} R(s_1, x_{3,0}, \tau - \tau') \times f_1^+(s_1, x_{3,0}, x_{3,F}, \tau') d\tau' \quad (69)$$

and

$$M^+(s_1, x_{3,0}, x_{3,F}, -\tau) = w^+(s_1, \tau) \int_{-\infty}^{\tau} R(s_1, x_{3,0}, \tau - \tau') \times f_1^-(s_1, x_{3,0}, x_{3,F}, -\tau') d\tau', \quad (70)$$

with $f_1^+(s_1, x_{3,0}, x_{3,F}, \tau)$ defined in Eq. (66). This system of equations can be solved by the following iterative scheme:

$$f_{1,k}^-(s_1, x_{3,0}, x_{3,F}, \tau) = w^-(s_1, \tau) \int_{-\infty}^{\tau} R(s_1, x_{3,0}, \tau - \tau') \times f_{1,k}^+(s_1, x_{3,0}, x_{3,F}, \tau') d\tau' \quad (71)$$

and

$$M_{k+1}^+(s_1, x_{3,0}, x_{3,F}, -\tau) = w^+(s_1, \tau) \int_{-\infty}^{\tau} R(s_1, x_{3,0}, \tau - \tau') \times f_{1,k}^-(s_1, x_{3,0}, x_{3,F}, -\tau') d\tau', \quad (72)$$

with

$$f_{1,k}^+(s_1, x_{3,0}, x_{3,F}, \tau) = f_{1,d}^+(s_1, x_{3,0}, x_{3,F}, \tau) + M_k^+(s_1, x_{3,0}, x_{3,F}, \tau), \quad (73)$$

starting with $M_1^+(s_1, x_{3,0}, x_{3,F}, \tau) = 0$. Note that this scheme requires the measured reflection response $R(s_1, x_{3,0}, \tau)$ of the layered medium, estimates of the onset times $\tau_{\text{on}}^+(s_1)$ and $\tau_{\text{on}}^-(s_1)$, and an estimate of the direct arrival of the focusing function, $f_{1,d}^+(s_1, x_{3,0}, x_{3,F}, \tau)$. Assuming a background model of the medium is available, the primary downgoing and upgoing waves can be modelled, from which the onset times can be retrieved. Moreover, the direct arrival of the focusing function can be obtained, analogous to Eq. (59), from the direct arrival of the transmission response $\tilde{T}_d(s_1, x_{3,F}, x_{3,0}, \omega)$ (i.e., the modelled primary downgoing wave), according to

$$\tilde{f}_{1,d}^+(s_1, x_{3,0}, x_{3,F}, \omega) = \frac{\beta_3(x_{3,F}, \omega)}{2s_3(s_1, x_{3,F}, \omega) \tilde{T}_d(s_1, x_{3,F}, x_{3,0}, \omega)}, \quad (74)$$

followed by an inverse Fourier transform.

Once the iterative scheme has converged, the retrieved focusing functions can be used in the representations from Eqs. (64) and (65) to obtain the decomposed Green's functions $G^-(s_1, x_{3,F}, x_{3,0}, \tau)$ and $G^+(s_1, x_{3,F}, x_{3,0}, \tau)$ and, finally, the total Green's function $G(s_1, x_{3,F}, x_{3,0}, \tau) = G^+(s_1, x_{3,F}, x_{3,0}, \tau) + G^-(s_1, x_{3,F}, x_{3,0}, \tau)$. Note that the latter can be interpreted as the response to a source at the surface $x_{3,0}$, observed by a virtual receiver at $x_{3,F}$ inside the medium. Using reciprocity, $G(s_1, x_{3,0}, x_{3,F}, \tau)$ can be interpreted as the response to a virtual source at $x_{3,F}$ inside the medium, observed by a receiver at $x_{3,0}$. The retrieved Green's function contains the direct arrival and the primary and multiple reflections of the layered medium. The direct arrival comes from the background model whereas the primary and multiple reflections come from the measured reflection response at the surface.

Next, we show how to obtain the response between a virtual source and a virtual receiver, both inside the medium. To this end, note that the decomposed Green's functions are mutually related via^{60,61}

$$G^-(s_1, x_{3,F}, x_{3,0}, \tau) = \int_{-\infty}^{\tau} R(s_1, x_{3,F}, \tau - \tau') \times G^+(s_1, x_{3,F}, x_{3,0}, \tau') d\tau', \quad (75)$$

where $R(s_1, x_{3,F}, \tau)$ is the reflection response at depth level $x_{3,F}$ of the medium below this depth level, assuming a homogeneous medium above this depth level. By inverting Eq. (75), which is done by deconvolution, $R(s_1, x_{3,F}, \tau)$ is obtained from $G^-(s_1, x_{3,F}, x_{3,0}, \tau)$ and $G^+(s_1, x_{3,F}, x_{3,0}, \tau)$. This deconvolution process removes all the multiple reflections occurring in the medium above $x_{3,F}$. The retrieved reflection response $R(s_1, x_{3,F}, \tau)$ can be interpreted as the response to a virtual source for downgoing waves at $x_{3,F}$, observed by a virtual receiver for upgoing waves at $x_{3,F}$.

V. NUMERICAL EXAMPLE

We illustrate the Marchenko method with a numerical example for a horizontally layered acoustic medium consisting of a mix of DPS and DNG layers (see Fig. 6). All layers are homogeneous and isotropic, with $\beta_1 = \beta_3 = \beta$, where β stands for the mass density (see Table I).

The DPS layers consist of natural non-dispersive materials with $h_x(\omega) = h_\beta(\omega) = 1$. Hence, according to Eqs. (7) and (8), the layer parameters simplify to $\alpha(\omega) = \alpha_0$ and $\beta(\omega) = \beta_0$. In Fig. 6, the parameters of the DPS layers are the mass density β_0 and the phase velocity $c_0 = (\alpha_0\beta_0)^{-1/2}$.

The DNG layers consist of dispersive metamaterials. For these layers, we use the Drude model of Eqs. (9) and (10), with $\omega_x = \omega_\beta = \omega_0$ and $\Gamma_x = \Gamma_\beta = \Gamma$. Hence, $h_x(\omega) = h_\beta(\omega) = h(\omega) = 1 - \omega_0^2/[\omega(\omega + i\Gamma)]$. For low frequencies ($\omega \ll \omega_0$), this is approximated by $h(\omega) = -\omega_0^2/[\omega(\omega + i\Gamma)]$. Using Eqs. (7) and (8), we write

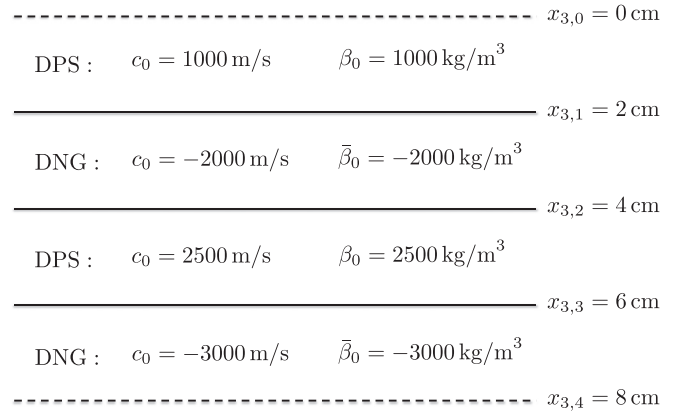


FIG. 6. Layered acoustic medium, consisting of DPS and DNG layers.

$$\alpha(\omega) = \alpha_0 h(\omega) = \bar{\alpha}_0 \bar{h}(\omega), \quad (76)$$

$$\beta(\omega) = \beta_0 h(\omega) = \bar{\beta}_0 \bar{h}(\omega), \quad (77)$$

with

$$\bar{\alpha}_0 = -\alpha_0 \frac{\omega_0^2}{\omega_c^2} < 0, \quad (78)$$

$$\bar{\beta}_0 = -\beta_0 \frac{\omega_0^2}{\omega_c^2} < 0, \quad (79)$$

$$\bar{h}(\omega) = -h(\omega) \frac{\omega_c^2}{\omega_0^2} = \frac{\omega_c^2}{\omega(\omega + i\Gamma)}, \quad (80)$$

where ω_c is the central angular frequency of the wave fields that will be considered. For consistency with the low frequency assumption, we assume $\omega_c \ll \omega_0$. In Fig. 6, the parameters of the DNG layers are the mass density $\bar{\beta}_0$ and the phase velocity $c_0 = -(\bar{\alpha}_0\bar{\beta}_0)^{-1/2}$. The parameter Γ in the DNG layers is set to $\Gamma = \omega_c/1000$.

We consider a band-limited ultrasonic downgoing plane wave, incident to the layered medium at $x_{3,0} = 0$ cm. The source function of the incident wave is defined as $S(\tau) = (1 - \omega_c^2\tau^2/2) \exp(-\omega_c^2\tau^2/4)$ (a so-called Ricker wavelet), with a central frequency $\omega_c/2\pi = 500$ kHz. Note that this wavelet is symmetric in time. We use a wavenumber-frequency domain modelling method,⁶² adjusted for metamaterials, to model the response to this plane wave. For the moment we consider vertically propagating plane waves, hence, we take $s_1 = 0$. The modelled reflection response $R(s_1 = 0, x_{3,0}, \tau)$, convolved with the wavelet $S(\tau)$, is shown in Fig. 7(a). This figure clearly shows the non-dispersed reflection at 40 μ s from the first layer interface at $x_{3,1} = 2$ cm. It also shows the dispersed reflections from deeper interfaces, including multiple reflections between the interfaces. Figure 7(b) is the modelled Green's function $G(s_1 = 0, x_3, x_{3,0}, \tau)$ inside the medium, as a function of depth x_3 and time τ . This serves as a reference for the results we will obtain with the Marchenko method. To make the later arrivals visible, a time-dependent amplitude gain of $\exp(2.5\tau/\tau_{\max})$, with $\tau_{\max} = 140 \mu$ s, has been applied in

this display. This figure shows how the wave field propagates through the layers and scatters at the interfaces. The downward and upward pointing arrows in the deepest layer indicate the opposite group and phase propagation directions. The upward propagating part of the upper trace in this figure is proportional to the reflection response $R(s_1 = 0, x_{3,0}, \tau)$ [see Eq. (55)], which is shown separately in Fig. 7(a). Similarly, the lower trace is proportional to the transmission response $T(s_1 = 0, x_{3,4}, x_{3,0}, \tau)$, with $x_{3,4} = 8$ cm, which is shown separately in Fig. 7(c). The trace at $x_3 = 5$ cm is equal to the superposition of Figs. 5(a) and 5(c). Figure 7(d) shows the power flux density $j(x_3)$, defined in Eq. (32), divided by $j(x_{3,0})$. In the DNG layers, it decreases because $\Gamma \neq 0$ in these layers. In a lossless medium, $j(x_3)$ would be constant, i.e., propagation invariant. Its deviation from being constant implies that the Marchenko method, which is based on propagation invariants, cannot lead to exact results. Since in this example the losses are small, the effects on the results of the Marchenko method are limited.

We use the Marchenko method discussed in Sec. IV to retrieve the Green's function $G(s_1 = 0, x_{3,F}, x_{3,0}, \tau)$ inside the medium from the reflection response $R(s_1 = 0, x_{3,0}, \tau)$, shown in Fig. 7(a). Apart from the reflection response, we also need an estimate of the direct arrival of the focusing function, $f_{1,d}^+(s_1 = 0, x_{3,0}, x_{3,F}, \tau)$, which, according to Eq. (74), follows from the inverse of the direct arrival of the transmission response. For this direct arrival, we need a background model of the medium. For the moment, we use the exact model, but in a later example, we replace it by an approximate model. Figure 8(a) shows $f_{1,d}^+(s_1 = 0, x_{3,0}, x_{3,F}, -\tau)$ [convolved with the symmetric wavelet $S(\tau)$] for variable $x_{3,F}$. The trace at $x_{3,F} = 5$ cm is equal to the direct arrival of the time-reversed focusing function in Fig. 5(b). Given the reflection response at the surface [Fig. 7(a)], the time-reversed direct arrival of the focusing function [Fig. 8(a)], and the depth-dependent onset times τ_{on}^+ and τ_{on}^- , we apply the iterative Marchenko scheme of Eqs. (71)–(73) for 64 focal depths, ranging from $x_{3,F} = 1.25$ mm to $x_{3,F} = 8$ cm, with steps $\Delta x_{3,F} = 1.25$ mm. For the window w^- in Eq. (71), we use a cosine-square taper with a length of $8\pi/\omega_c$ s (except in the upper DPS layer, where we replace this window by w^+). The length of the taper appears to have no strong effect on the results of the method. For each focal depth $x_{3,F}$, we apply five iterations. Actually, for this relatively simple situation, the method converges already after two iterations and it remains stable even after 100 iterations. The obtained focusing functions $f_1^-(s_1 = 0, x_{3,0}, x_{3,F}, \tau)$ and $f_1^+(s_1 = 0, x_{3,0}, x_{3,F}, \tau)$ are subsequently used in Eqs. (64) and (65) to obtain the Green's functions $G^-(s_1 = 0, x_{3,F}, x_{3,0}, \tau)$ and $G^+(s_1 = 0, x_{3,F}, x_{3,0}, \tau)$. These are shown in Figs. 8(b) and 8(c) for variable $x_{3,F}$. Superposing these results yields the total Green's function $G(s_1 = 0, x_{3,F}, x_{3,0}, \tau)$ [see Fig. 9(a)]. Figure 9(b) shows the difference of this retrieved Green's function with the directly modelled Green's function in Fig. 7(b) (the same time-dependent amplitude gain has been applied in this display as in the other figures). Note

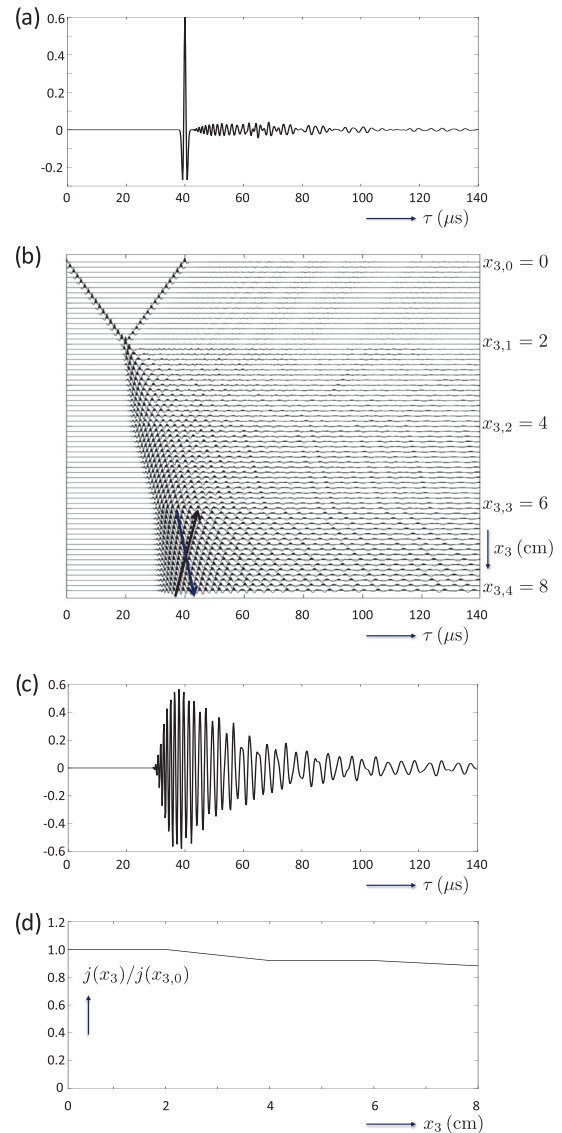


FIG. 7. Modelled wave field in the layered medium of Fig. 6. (a) Reflection response $R(s_1 = 0, x_{3,0}, \tau)$. (b) Green's function $G(s_1 = 0, x_3, x_{3,0}, \tau)$. (c) Transmission response $T(s_1 = 0, x_{3,4}, x_{3,0}, \tau)$. (d) Power flux density as a function of x_3 .

that the difference is overall small. This is also seen in Fig. 9(c), which shows a comparison of the directly modelled and retrieved Green's functions at $x_{3,F} = 5$ cm. The phases match very well and the amplitudes deviate typically a few percent, with some outliers in the order of 10%. From the decomposed Green's functions, we can retrieve the reflection response $R(s_1 = 0, x_{3,F}, \tau)$ for any $x_{3,F}$ by inverting Eq. (75). The retrieved response for $x_{3,F} = 5$ cm is shown in Fig. 9(d). This is the reflection response of the third interface at $x_{3,3} = 6$ cm in Fig. 6, measured with a virtual source and a virtual receiver 1 cm above this interface. We observe a single primary reflection event at 8.0μ s; the dispersion effects of the overlying DNG layer and the multiple reflections occurring in the medium above $x_{3,F}$ have been properly removed (apart from a very small remnant of a multiple reflection at approximately 24.0μ s). The amplitude of the reflection

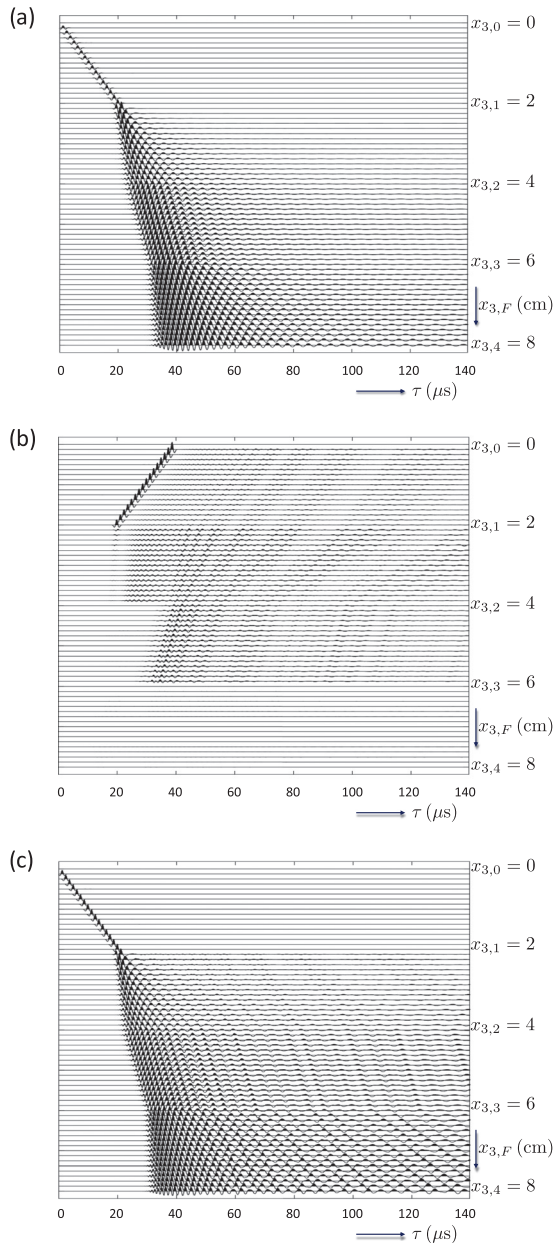


FIG. 8. Wavefield retrieval with the Marchenko method. (a) Time-reversed direct arrival of the focusing function, $f_{1,d}^+(s_1 = 0, x_{3,0}, x_{3,F}, -\tau)$. (b) Retrieved upgoing Green's function $G^-(s_1 = 0, x_{3,F}, x_{3,0}, \tau)$. (c) Retrieved downgoing Green's function $G^+(s_1 = 0, x_{3,F}, x_{3,0}, \tau)$.

event at $8.0 \mu\text{s}$ is 0.159, which is a slight underestimation of the true reflection coefficient $r_3 = 0.180$ for $\omega = \omega_c$. This discrepancy is due to the loss occurring in the DNG layer between $x_{3,1} = 2 \text{ cm}$ and $x_{3,2} = 4 \text{ cm}$.

To emphasize what we have achieved with the Marchenko method, we repeat this numerical experiment with a method that handles primaries only (to this end, we use the same method as before, but apply zero iterations for each focal depth). Figure 10(a) shows the retrieved Green's function $G(s_1 = 0, x_{3,F}, x_{3,0}, \tau)$ and Fig. 10(b) shows the difference with the directly modelled Green's function in Fig. 7(b). Note that this difference is significantly stronger than that in Fig. 9(b). Figure 10(c) shows again a comparison of

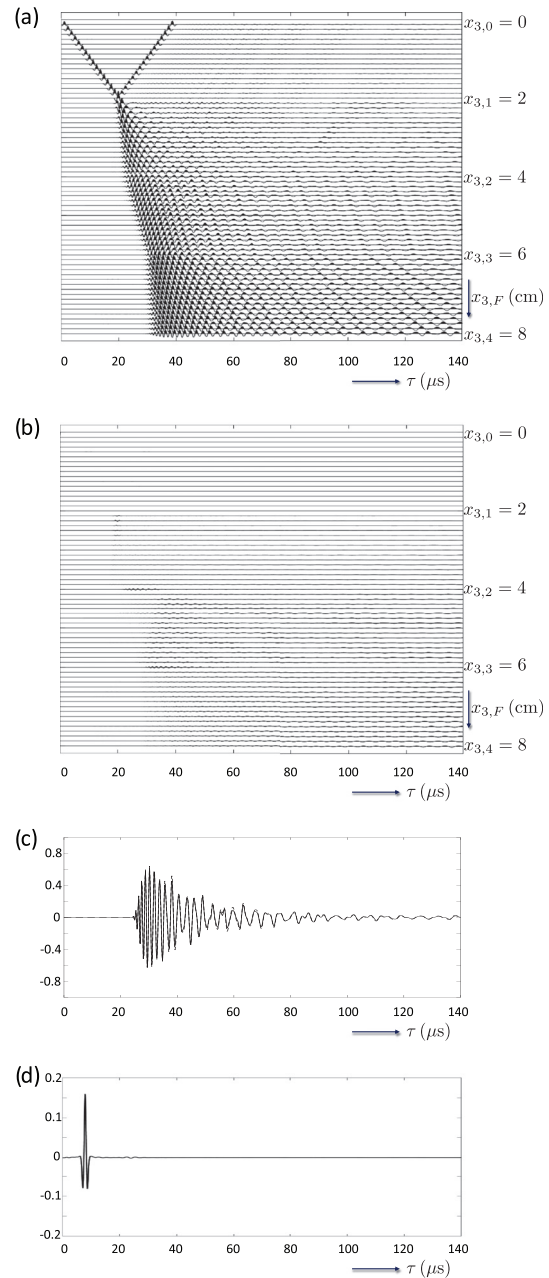


FIG. 9. Wavefield retrieval with the Marchenko method (continued). (a) Total retrieved Green's function $G(s_1 = 0, x_{3,F}, x_{3,0}, \tau) = G^+(s_1 = 0, x_{3,F}, x_{3,0}, \tau) + G^-(s_1 = 0, x_{3,F}, x_{3,0}, \tau)$. (b) Difference of the retrieved Green's function with the directly modelled Green's function of Fig. 7(b). (c) Overlay of directly modelled (solid) and retrieved (dashed) Green's functions at $x_{3,F} = 5 \text{ cm}$. (d) Retrieved reflection response $R(s_1 = 0, x_{3,F}, \tau)$ at $x_{3,F} = 5 \text{ cm}$ of the interface at $x_{3,3} = 6 \text{ cm}$.

the directly modelled and retrieved Green's functions at $x_{3,F} = 5 \text{ cm}$. Figure 10(d) shows the retrieved reflection response $R(s_1 = 0, x_{3,F}, \tau)$ for $x_{3,F} = 5 \text{ cm}$, obtained by inverting Eq. (75). The amplitude of the retrieved reflection event at $8.0 \mu\text{s}$ is now 0.096, almost a factor 2 too low. Moreover, the events directly following this reflection event are caused by multiple reflections in the medium above $x_{3,F} = 5 \text{ cm}$, which obviously have not been removed by this method.

In practice, we do not know the exact model, so we can obtain only an estimate of the direct arrival of the focusing function and of the onset times τ_{on}^+ and τ_{on}^- . We apply the same Marchenko method as above (again with five iterations for each focal depth), but this time we use erroneous phase velocities c_0 of 975, -2050, 2550, and -2950 m/s in the four layers (and the same numerical values for the mass density). Because of the erroneous velocities, the travel times of the retrieved Green's functions are erroneous as well, but the multiple reflections are correctly handled.⁶³ Figure 11(a) shows the retrieved reflection response $R(s_1 = 0, x_{3,F}, \tau)$ for $x_{3,F} = 5$ cm. We observe a single reflection event at 7.6 μs

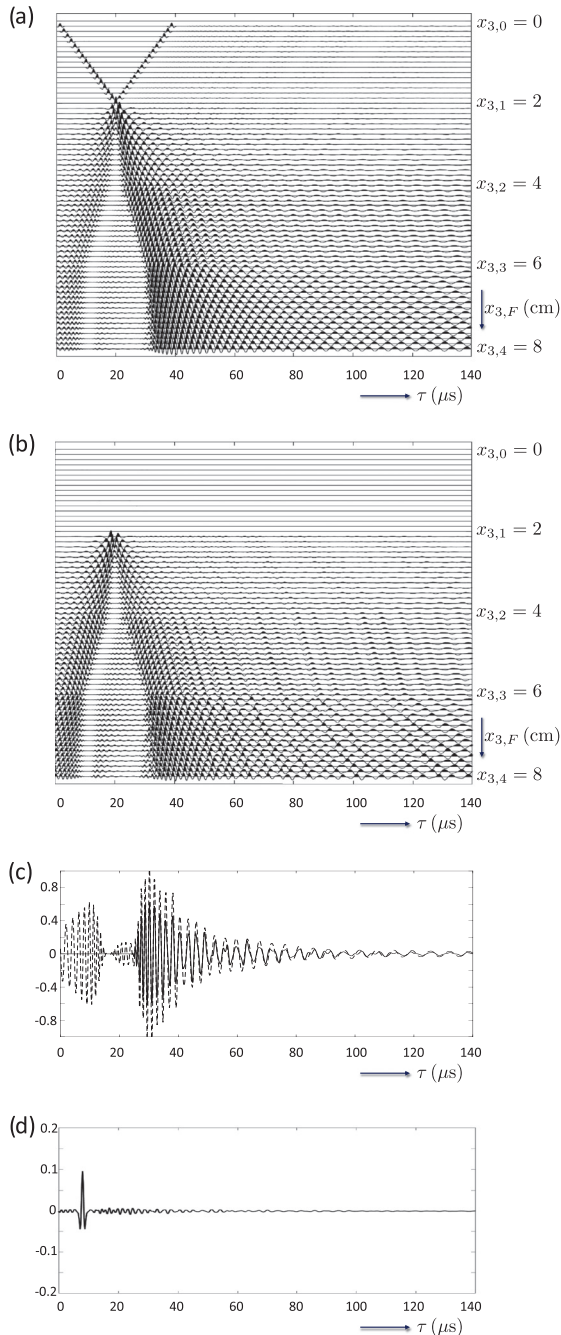


FIG. 10. As Fig. 9, but using a method that handles primaries only.

and hardly any remnants of multiples, which confirms that the multiple reflections occurring in the medium above $x_{3,F}$ have again been properly removed. The phase of the reflection event is distorted, but the envelope (indicated by the dashed line) has a peak value of 0.149, which still approximates the true reflection coefficient $r_3 = 0.180$ reasonably well.

Finally, we repeat the numerical experiment, using the same erroneous phase velocities, for a dipping plane wave with a small non-zero horizontal slowness $s_1 = 40 \mu\text{s/m}$. The propagation angle α for $\omega = \omega_c$ is related to the slowness s_1 and the phase velocities c_0 of the different layers via $\alpha = \arcsin(s_1 c_0)$. For $s_1 = 40 \mu\text{s/m}$, the angles in the four layers of Fig. 6 are 2.29° , -4.59° , 5.74° and -6.89° , respectively. The retrieved reflection response $R(s_1, x_{3,F}, \tau)$ for $s_1 = 40 \mu\text{s/m}$ and $x_{3,F} = 5$ cm is shown in Fig. 11(b). The amplitude of the retrieved reflection response of the third interface is 0.157, which is a reasonable approximation of the true reflection coefficient $r_3 = 0.181$ for $\omega = \omega_c$ and $s_1 = 40 \mu\text{s/m}$.

VI. CONCLUDING REMARKS

We have shown that the Marchenko method, which retrieves the wavefield inside a medium from its reflection response at the surface, can be extended for metamaterials. The main modification is the use of a new window function, which better accounts for the strong dispersive behaviour of waves in metamaterials. The method holds in the low frequency limit for elastodynamic and electromagnetic waves in layered media, consisting of a mix of natural materials and metamaterials. Multiple scattering between the layer interfaces is properly taken into account. We have shown with a numerical example that the method accurately retrieves the response to a source at the surface, observed by virtual receivers inside the medium. By deconvolving the retrieved upgoing field by the retrieved downgoing field, we

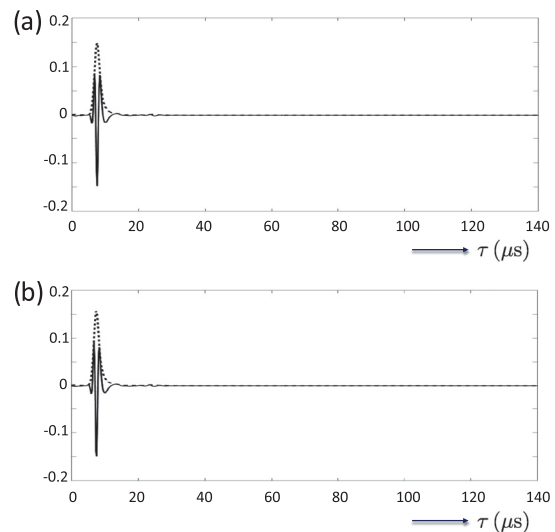


FIG. 11. (a) As Fig. 9(d), but using erroneous phase velocities. (b) As Fig. 9(d), but for $s_1 = 40 \mu\text{s/m}$ and using erroneous phase velocities.

accurately obtain the reflection response between a virtual source and a virtual receiver, both inside the medium.

The method works well for vertically propagating plane waves and for dipping plane waves with small horizontal slownesses, corresponding to propagation angles up to approximately 7° . For larger horizontal slownesses, the method becomes unstable. Due to the strong dispersive behaviour of the DNG layers, the propagation angle for a fixed horizontal slowness is frequency-dependent and can become post-critical for high frequencies, which explains the unstable behaviour. A possible remedy is to remove the high frequencies from the source spectrum, but this will go at the cost of resolution. Further research is needed to optimize the proposed method for a wider range of propagation angles.

Whereas we only considered horizontally layered media, in principle, the method can be extended for laterally varying metamaterials in a similar way as for natural materials.⁶³ The strong dispersive character of metamaterials will limit the maximum aperture angle of the space-time focusing operators and hence the obtainable lateral resolution. An interesting option to be investigated further is the virtual plane-wave Marchenko approach for laterally varying media,⁶⁴ modified for metamaterials.

The proposed method can potentially be used in any application of metamaterials where knowledge of the wavefield inside the medium is required, for example, in non-destructive testing of layered materials, where anomalies of the retrieved reflectivity may be used to determine the location of a delamination.

ACKNOWLEDGMENTS

The constructive comments of Patrick Elison and an anonymous reviewer are highly appreciated. This work has received funding from the European Union's Horizon 2020 research and innovation programme: European Research Council (Grant Agreement 742703).

¹V. A. Marchenko, "Reconstruction of the potential energy from the phases of the scattered waves (in Russian)," *Dokl. Akad. Nauk SSSR* **104**, 695–698 (1955).

²G. L. Lamb, *Elements of Soliton Theory* (John Wiley and Sons, Inc., New York, 1980), pp. 46–67.

³K. Chadan and P. C. Sabatier, *Inverse Problems in Quantum Scattering Theory* (Springer, Berlin, 1989), Chaps. 5 and 7.

⁴D. E. Budreck and J. H. Rose, "Three-dimensional inverse scattering in anisotropic elastic media," *Inverse Probl.* **6**, 331–348 (1990).

⁵J. H. Rose, "'Single-sided' focusing of the time-dependent Schrödinger equation," *Phys. Rev. A* **65**, 012707 (2001).

⁶J. H. Rose, "'Single-sided' autofocusing of sound in layered materials," *Inverse Probl.* **18**, 1923–1934 (2002).

⁷F. Broggin, R. Snieder, "Connection of scattering principles: A visual and mathematical tour," *Eur. J. Phys.* **33**, 593–613 (2012).

⁸K. Wapenaar, F. Broggin, and R. Snieder, "Creating a virtual source inside a medium from reflection data: Heuristic derivation and stationary-phase analysis," *Geophys. J. Int.* **190**, 1020–1024 (2012).

⁹J. Van der Neut, I. Vasconcelos, and K. Wapenaar, "On Green's function retrieval by iterative substitution of the coupled Marchenko equations," *Geophys. J. Int.* **203**, 792–813 (2015).

¹⁰P. Elison, D. J. van Manen, J. O. A. Robertsson, M. S. Dukalski, and K. de Vos, "Marchenko-based immersive wave simulation," *Geophys. J. Int.* **215**, 1118–1131 (2018).

¹¹K. Wapenaar, J. Brackenhoff, J. Thorbecke, J. van der Neut, E. Slob, and E. Verschuur, "Virtual acoustics in inhomogeneous media with single-sided access," *Sci. Rep.* **8**, 2497 (2018).

¹²M. Dukalski and K. de Vos, "Marchenko inversion in a strong scattering regime including surface-related multiples," *Geophys. J. Int.* **212**, 760–776 (2018).

¹³J. Brackenhoff, J. Thorbecke, and K. Wapenaar, "Monitoring of induced distributed double-couple sources using Marchenko-based virtual receivers," *Solid Earth* **10**, 1301–1319 (2019).

¹⁴K. Wapenaar, J. Thorbecke, J. van der Neut, F. Broggin, E. Slob, and R. Snieder, "Marchenko imaging," *Geophysics* **79**, WA39–WA57 (2014).

¹⁵E. Slob, K. Wapenaar, F. Broggin, and R. Snieder, "Seismic reflector imaging using internal multiples with Marchenko-type equations," *Geophysics* **79**, S63–S76 (2014).

¹⁶F. Broggin, R. Snieder, and K. Wapenaar, "Data-driven wavefield focusing and imaging with multidimensional deconvolution: Numerical examples for reflection data with internal multiples," *Geophysics* **79**, WA107–WA115 (2014).

¹⁷G. A. Meles, K. Löer, M. Ravasi, A. Curtis, and C. A. da Costa Filho, "Internal multiple prediction and removal using Marchenko autofocusing and seismic interferometry," *Geophysics* **80**, A7–A11 (2015).

¹⁸M. Ravasi, I. Vasconcelos, A. Kritski, A. Curtis, C. A. da Costa Filho, and G. A. Meles, "Target-oriented Marchenko imaging of a North Sea field," *Geophys. J. Int.* **205**, 99–104 (2016).

¹⁹J. Van der Neut, M. Ravasi, Y. Liu, and I. Vasconcelos, "Target-enclosed seismic imaging," *Geophysics* **82**, Q53–Q66 (2017).

²⁰C. Mildner, F. Broggin, J. O. A. Robertsson, D. J. van Manen, and S. Greenhalgh, "Target-oriented velocity analysis using Marchenko-redatumed data," *Geophysics* **82**, R75–R86 (2017).

²¹M. Ravasi, "Rayleigh-Marchenko redatuming for target-oriented, true-amplitude imaging," *Geophysics* **82**, S439–S452 (2017).

²²M. Staring, R. Pereira, H. Douma, J. van der Neut, and K. Wapenaar, "Source-receiver Marchenko redatuming on field data using an adaptive double-focusing method," *Geophysics* **83**, S579–S590 (2018).

²³K. Wapenaar and C. Reinicke, "Unified wave field retrieval and imaging method for inhomogeneous non-reciprocal media," *J. Acoust. Soc. Am.* **146**, 810–825 (2019).

²⁴V. G. Veselago, "The electrodynamics of substances with simultaneously negative values of ϵ and μ ," *Soviet Phys. Uspekhi* **10**, 509–514 (1968).

²⁵J. B. Pendry, "Negative refraction makes a perfect lens," *Phys. Rev. Lett.* **85**, 3966–3969 (2000).

²⁶R. W. Ziolkowski and E. Heyman, "Wave propagation in media having negative permittivity and permeability," *Phys. Rev. E* **64**, 056625 (2001).

²⁷R. Marqués, F. Medina, and R. Rafii-El-Idrissi, "Role of bianisotropy in negative permeability and left-handed metamaterials," *Phys. Rev. B* **65**, 144440 (2002).

²⁸R. W. Ziolkowski and A. D. Kipple, "Causality and double-negative metamaterials," *Phys. Rev. E* **68**, 026615 (2003).

²⁹R. W. Ziolkowski, "Pulsed and CW Gaussian beam interactions with double negative metamaterial slabs," *Opt. Exp.* **11**, 662–681 (2003).

³⁰N. Engheta and R. W. Ziolkowski, *Metamaterials: Physics and Engineering Explorations* (John Wiley and Sons, Inc., New York, 2006), Chap. 1.

³¹D. R. Smith and J. B. Pendry, "Homogenization of metamaterials by field averaging (invited paper)," *J. Opt. Soc. Am. B* **23**, 391–403 (2006).

³²N. Yu, P. Genevet, M. A. Kats, F. Aieta, J.-F. Tetienne, F. Capasso, and Z. Gaburro, "Light propagation with phase discontinuities: Generalized laws of reflection and refraction," *Science* **334**, 333–337 (2011).

³³J. R. Willis, "Effective constitutive relations for waves in composites and metamaterials," *Proc. R. Soc. A* **467**, 1865–1879 (2011).

³⁴J. Nemirovsky, M. C. Rechtsman, and M. Segev, "Negative radiation pressure and negative effective refractive index via dielectric birefringence," *Opt. Express* **20**, 8907–8914 (2012).

³⁵Z. Liu, X. Zhang, Y. Mao, Y. Y. Zhu, Z. Yang, C. T. Chan, and P. Sheng, "Locally resonant sonic materials," *Science* **289**, 1734–1736 (2000).

³⁶Z. Liu, C. T. Chan, and P. Sheng, "Analytic model of phononic crystals with local resonances," *Phys. Rev. B* **71**, 014103 (2005).

³⁷S. Guenneau, A. Movchan, G. Pétursson, and S. A. Ramakrishna, "Acoustic metamaterials for sound focusing and confinement," *New J. Phys.* **9**, 399 (2007).

- ³⁸A. N. Norris, "Acoustic metafluids," *J. Acoust. Soc. Am.* **125**, 839–849 (2009).
- ³⁹J. R. Willis, "The construction of effective relations for waves in a composite," *C. R. Mec.* **340**, 181–192 (2012).
- ⁴⁰R. Zhu, X. N. Liu, G. L. Huang, H. Huang, and C. T. Sun, "Microstructural design and experimental validation of elastic metamaterial plates with anisotropic mass density," *Phys. Rev. B* **86**, 144307 (2012).
- ⁴¹A. P. Liu, R. Zhu, X. N. Liu, G. K. Hu, and G. L. Huang, "Multi-displacement microstructure continuum modeling of anisotropic elastic metamaterials," *Wave Motion* **49**, 411–426 (2012).
- ⁴²A. N. Norris, A. L. Shuvalov, and A. A. Kutsenko, "Analytical formulation of three-dimensional dynamic homogenization for periodic elastic systems," *Proc. R. Soc. A* **468**, 1629–1651 (2012).
- ⁴³Z. Liang and J. Li, "Extreme acoustic metamaterial by coiling up space," *Phys. Rev. Lett.* **108**, 114301 (2012).
- ⁴⁴M. R. Haberman and M. D. Guild, "Acoustic metamaterials," *Phys. Today* **69**(6), 42–48 (2016).
- ⁴⁵H. Nassar, H. Chen, A. N. Norris, M. R. Haberman, and G. L. Huang, "Non-reciprocal wave propagation in modulated elastic metamaterials," *Proc. R. Soc. A* **473**, 20170188 (2017).
- ⁴⁶W. T. Thomson, "Transmission of elastic waves through a stratified solid medium," *J. Appl. Phys.* **21**, 89–93 (1950).
- ⁴⁷N. A. Haskell, "The dispersion of surface waves on multilayered media," *Bull. Seismol. Soc. Am.* **43**, 17–34 (1953).
- ⁴⁸J. P. Coron, "Bremmer series that correct parabolic approximations," *J. Math. Anal. Appl.* **50**, 361–372 (1975).
- ⁴⁹B. Ursin, "Review of elastic and electromagnetic wave propagation in horizontally layered media," *Geophysics* **48**, 1063–1081 (1983).
- ⁵⁰L. Fishman and J. J. McCoy, "Derivation and application of extended parabolic wave theories. I. The factorized Helmholtz equation," *J. Math. Phys.* **25**, 285–296 (1984).
- ⁵¹M. V. de Hoop, "Generalization of the Bremmer coupling series," *J. Math. Phys.* **37**, 3246–3282 (1996).
- ⁵²K. Wapenaar, "Unified matrix-vector wave equation, reciprocity and representations," *Geophys. J. Int.* **216**, 560–583 (2019).
- ⁵³C. P. A. Wapenaar and A. J. Berkhout, *Elastic Wave Field Extrapolation* (Elsevier, Amsterdam, 1989), Chap. 3.
- ⁵⁴A. J. Haines, "Multi-source, multi-receiver synthetic seismograms for laterally heterogeneous media using F-K domain propagators," *Geophys. J. Int.* **95**, 237–260 (1988).
- ⁵⁵B. L. N. Kennett, K. Koketsu, and A. J. Haines, "Propagation invariants, reflection and transmission in anisotropic, laterally heterogeneous media," *Geophys. J. Int.* **103**, 95–101 (1990).
- ⁵⁶K. Koketsu, B. L. N. Kennett, and H. Takenaka, "2-D reflectivity method and synthetic seismograms for irregularly layered structures—II. Invariant embedding approach," *Geophys. J. Int.* **105**, 119–130 (1991).
- ⁵⁷H. Takenaka, B. L. N. Kennett, and K. Koketsu, "The integral operator representation of propagation invariants for elastic waves in irregularly layered media," *Wave Motion* **17**, 299–317 (1993).
- ⁵⁸K. Wapenaar, F. Broggini, E. Slob, and R. Snieder, "Three-dimensional single-sided Marchenko inverse scattering, data-driven focusing, Green's function retrieval, and their mutual relations," *Phys. Rev. Lett.* **110**, 084301 (2013).
- ⁵⁹P. L. Stoffa, *Tau-p—A Plane Wave Approach to the Analysis of Seismic Data* (Kluwer Academic Publishers, Dordrecht) (1989), p. 15.
- ⁶⁰K. Wapenaar, J. Fokkema, M. Dillen, and P. Scherpenhuijsen, "One-way acoustic reciprocity and its applications in multiple elimination and time-lapse seismics," in *SEG, Expanded Abstracts* (SEG, Tulsa, OK, 2000), pp. 2377–2380.
- ⁶¹L. Amundsen, "Elimination of free-surface related multiples without need of the source wavelet," *Geophysics* **66**, 327–341 (2001).
- ⁶²B. L. N. Kennett and N. J. Kerry, "Seismic waves in a stratified half-space," *Geophys. J. R. Astron. Soc.* **57**, 557–584 (1979).
- ⁶³K. Wapenaar, J. Thorbecke, J. van der Neut, F. Broggini, E. Slob, and R. Snieder, "Green's function retrieval from reflection data, in absence of a receiver at the virtual source position," *J. Acoust. Soc. Am.* **135**, 2847–2861 (2014).
- ⁶⁴G. A. Meles, K. Wapenaar, and J. Thorbecke, "Virtual plane-wave imaging via Marchenko redatuming," *Geophys. J. Int.* **214**, 508–519 (2018).